Glucose determination in human aqueous humor with Raman spectroscopy

James L. Lambert
Christine C. Pelletier
Jet Propulsion Laboratory
California Institute of Technology
Pasadena, California 91109-8099

Mark Borchert
University of Southern California
Division of Ophthalmology
Children Hospital Los Angeles
and
Department of Ophthalmology
Keck School of Medicine
Los Angeles, California

Abstract. It has been suggested that spectroscopic analysis of the aqueous humor of the eye could be used to indirectly predict blood glucose levels in diabetics noninvasively. We have been investigating this potential using Raman spectroscopy in combination with partial least squares (PLS) analysis. We have determined that glucose at clinically relevant concentrations can be accurately predicted in human aqueous humor *in vitro* using a PLS model based on artificial aqueous humor. We have further determined that with proper instrument design, the light energy necessary to achieve clinically acceptable prediction of glucose does not damage the retinas of rabbits and can be delivered at powers below internationally acceptable safety limits. Herein we summarize our current results and address our strategies to improve instrument design. [DOI: 10.1117/1.1914843]

Keywords: glucose; ocular; Raman spectroscopy; diabetes; non-invasive; aqueous humor; optical toxicity; partial least squares.

Paper SS04155R received Aug. 3, 2004; revised manuscript received Oct. 4, 2004; accepted for publication Oct. 5, 2004; published online Jun. 7, 2005.

Introduction

Optical sensors for determining glucose levels in biological fluids have been under investigation for at least three decades.[1–4] The 1993 report of the Diabetes Control and Complications Trial boosted this effort by underscoring the importance of frequent blood glucose monitoring for the effective management of diabetes mellitus.[5,6] Since over 18 million people in the United States alone (as of 2002) are estimated to have this disease,[7] researchers and small companies are attempting to develop less painful alternatives to the traditional finger-stick method for blood testing.[8–13] Many of these alternatives are based on near-infrared (NIR) absorption spectroscopy of blood-containing tissue (e.g., finger, earlobe, lip). Multivariate statistical techniques applied to NIR spectra have led to empirical correlations yielding quantitative glucose determinations under some conditions. However, repeatable and quantifiable results have been problematic *in vivo*. Difficulties include variability in the pathlength through pliable tissues and in the optical properties of those tissues, temperature variability, and the pulsatile nature of blood flow.[14]

Many have suggested that the aqueous humor in the anterior chamber of the eye could serve as a surrogate for blood for noninvasive spectroscopic analysis of glucose concentration. The aqueous humor in the anterior chamber of the eye is, optically, a more accessible glucose-containing body fluid. It is close to the surface, and the cornea is clear. We, and others, have suggested that glucose concentration in the aqueous humor may be particularly accessible by Raman spectroscopy.[15–17] Potential problems with such an approach include difficulties developing a model that is predictive over time in different individuals, risks of light toxicity to the eye, and practicality of using the instrument because of time or portability constraints. Herein we address the state of the art of noninvasive measurement of aqueous humor glucose using Raman spectroscopy and the technological hurdles that must be overcome to make this a useful technique in humans.

Address all correspondence to James L. Lambert, Jet Propulsion Laboratory, California Institute of Technology, 4800 Oak Grove Drive, M/S 300-123, Pasadena, CA 91109-8099. Tel: (818) 354-4181; Fax: (818) 393-3302; E-mail: James.L.Lambert@jpl.nasa.gov

Current Instrument Design

Our experience in Raman spectroscopy of glucose in aqueous humor uses the following custom-designed system. A Coherent Sabre argon laser is used to pump a Spectra Physics model 3900 Ti:sapphire laser using all lines at 5 W. An intercavity thin etalon is used to limit the spectral width of the Ti:sapphire laser to 80 MHz. The wavelength of the Ti:sapphire laser is set nominally to 785 nm using a Burleigh wavemeter (model WA-1100). A plasma line filter is used to remove fluorescence from the linearly polarized beam (p) and a $\frac{1}{2}$ wave plate is used to circularize the beam polarization prior to injection into a single-mode optical fiber. The fiber is coupled to a modified holographic Kaiser Raman probehead. Stress birefringence within the optical fiber can induce potentially large changes in the polarization of the beam that is subject to temperature drift and microphonics, and hence, difficult to control. For this reason, polarization optics are added within the probehead to convert the varying polarization state of the fiber-coupled light into one of a fixed and known state. A quartz prism is used to direct 5% of the beam to a detector that is used to measure the power delivered to the sample (or

1083-3668/2005/$22.00 © 2005 SPIE

subject). Holographic filters within the probehead are used to remove the Raman scattered light from silica within the excitation fiber.

The optical output of the probehead is directed through an Olympus BX60 microscope with an LCPlanFl 20× objective. Since the beam entering the objective does not fill the back aperture of the objective, the numerical aperture of the excitation beam in air is actually 0.0534. This was calculated by measuring the $1/e$ radius of the diverging output beam (106.87 mrad) at a fixed distance from the focal point of the objective using a knife-edge protocol.[18] A video charge coupled device (CCD) camera integrated with the Raman probehead is used to visualize the excitation beam on the sample.

The collected light from the sample is filtered by the holographic filters within probehead to remove most of the Rayleigh scattered light. Optics within the probehead confocally image the collection beam from the focal point of the objective onto a 50 μm metalized aperture evaporated onto the end of a gradient index multimode fiber. The output of the collection fiber is directed into a Kaiser $f/1.8$ Holospec spectrometer. A holographic notch filter removes any remaining Rayleigh scattered light. The Raman scattered light is then focused through a 50 μm wide slit. The output light from the slit is then recollimated and then diffracted by a Holoplex holographic grating onto an EEV 1024×256 element, backilluminated deep-depletion CCD detector array contained within a Princeton Instruments liquid nitrogen cooled camera (model LN/CCD-1024-EHRB/1). The grating disperses light onto upper and lower regions of the CCD corresponding to the lower (100–1900) and higher (1900–3500) Stokes-shifted wave number regimes.

The Raman spectrum of cyclohexane is used to determine the precise excitation wavelength of the Ti:sapphire laser. The wavemeter is also used to confirm this. The Kaiser Optic Systems calibration accessory is used to calibrate the CCD detector in terms of absolute wavelength using a neon source within the calibration accessory. The spectral responsiveness of the instrument is measured using the NBS traceable stabilized white light source within the calibration accessory.

Kaiser Holograms 4.0 software is used to control the detector electronics, which provide 16-bit resolution pixel data to the computer. A signal available on the camera controller provides a trigger signal for the shutter controller (Vincent VMM-D1) that limits exposure from the laser beam to the time during which a spectrum is being collected. Power measurements from the point detector on the probehead are measured by a Newport power meter (2832-C) and relayed to the computer via a serial interface. Matlab (Version 6.5) software is used to trigger operation of the Holograms Raman data acquisition and to continuously read power levels during sample exposure so that average power and energy can be determined.

Model Design

We have previously demonstrated that a clinically relevant range of glucose concentrations can be predicted in aqueous solutions using Raman spectroscopy combined with partial least squares (PLS) analysis.[19] We wished to determine if a PLS model generated from a set of aqueous solutions containing glucose and other metabolites in concentrations roughly equivalent to those that could be found in aqueous humor could predict glucose concentration from Raman spectra of natural human aqueous humor (HAH). If feasible, such a model using artificial aqueous humor (AAH) has several advantages. The necessity of collecting human aqueous humor to serve as a training set is avoided and a standardized set of AAH could be used for recalibration of any commercial instrument. Furthermore, a training set consisting of AAH avoids the possible covariance of some metabolites found in HAH. Avoiding covariance of metabolite concentrations is important for developing a robust PLS model.

A PLS model was developed using 50 AAH samples with independently varying concentrations of five major components (glucose [0–770 mg/dL], bicarbonate [0–250 mg/dL], lactate [0–200 mg/dL], urea [0–180 mg/dL], and ascorbate [0–90 mg/dL]) of human aqueous humor.[20] The concentrations of the constituents in each of the AAH solutions were selected such that the covariance between all components was zero using a coding scheme designed for the development of ideal chemometric models.[21] All solutions were prepared in 0.9% saline and pH was adjusted to 8 to correspond to the pH of HAH.[20]

A poly(methyl methacrylate) contact lens was filled with approximately 60 μL of sample solution, and then inverted onto a quartz microscope slide for Raman spectroscopy. This served as a model anterior chamber of the eye and was placed on a microscope stage beneath the objective lens of the Raman instrument.[19] The stage was advanced toward the objective lens until the surface of the contact lens was imaged on the video CCD camera and then an additional 1.1 mm so that the laser was focused in the middle of the aqueous sample.

Fifty 3 s spectra were acquired for each sample with laser power of 100 mW. These spectra were summed forming the equivalent of 150 s spectra. Exposures of 15 000 mJ were acquired in order to maximize signal-to-noise ratio (SNR) of the training spectra and thereby to realize a high fidelity PLS model that can then be used to predict glucose levels from spectra collected at lower energy, eye-safe exposures. The PLS model (using five factors) was calculated from the training spectra after selecting the 300–1500 wave number region, multiplicative signal correction, and mean centering. Leave-one-out cross validation resulted in a coefficient of determination (r^2) of 0.992, root-mean-squared-error of cross validation (RMSECV) of 24.0 mg/dL, and bias (mean difference between predicted and reference concentrations) of 0.3 mg/dL.

Current Results in Human Aqueous Humor

In a similar manner, spectra of 17 human aqueous humor *in vitro* samples were acquired. Six Raman spectra were collected using three second, ~100 mW (300 mJ) exposures for each sample of HAH. For each sample, these six spectra were summed to form the equivalent of one 18 s spectra (~1800 mJ), and tested against the PLS model developed from AAH. HAH samples were obtained with IRB approval from patients undergoing cataract surgery. Some samples were spiked with *D*-glucose to create a range of glucose concentration. Final glucose and lactate concentrations of the HAH samples were measured using a select biochemistry analyzer, model 2700

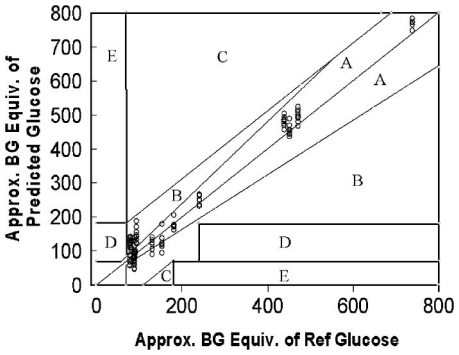

Fig. 1 Clarke grid. Glucose concentrations predicted from 18 s spectra of human aqueous humor have been approximately converted to blood glucose equivalent concentrations (divided by 0.7) and plotted versus a similar conversion of the reference AH glucose concentrations. For a given desired energy of exposure, the individual predictions for each sample are formed by summing the appropriate number of 3 s, 100 mW spectra, one right after the other. A high fidelity 50-AAH PLS model based on 150 s AAH spectra was used for prediction.

(YSI Life Sciences). The correlation coefficient of glucose and lactate levels in the HAH samples that were not spiked with glucose was $r=0.4$. Since the covariance of these two major constituents in human aqueous humor is nonzero, the use of HAH in PLS models may adversely affect their performance.

Glucose concentrations predicted from 18-s spectra of HAH samples are plotted on a Clarke grid[22] in Fig. 1 after an approximate conversion of aqueous humor glucose into blood glucose levels. The Clarke grid was originated as a tool to evaluate devices for patient self-monitoring of blood glucose. Results falling into regions A and B are considered clinically acceptable; those falling into regions C, D, and E are clinically unacceptable. Aqueous humor glucose concentration was converted into blood glucose concentration by dividing HAH glucose concentrations by 0.7. A ratio of 0.7 for human aqueous humor relative to blood glucose is suggested by the work of Pohjola[23] and of Schrader et al.[24] in which this ratio ranged from 0.65 to 0.76. There is some uncertainty in this conversion factor because aqueous humor glucose, but not blood glucose, may depend on age.[23] Pohjola's and Schrader's ratio values were determined from simultaneous AH and blood glucose measurements, while other research[2,15,25,26] suggests that there may be a delay of a few minutes before AH glucose equilibrates after changes in blood glucose.

The regional boundaries on a Clarke grid are based on several assumptions: (1) blood glucose should be between 70 and 180 mg/dL; (2) corrective action will be taken if blood glucose is ''predicted'' above 180 mg/dL; (3) $\pm 20\%$ deviation of predicted from reference blood glucose is always acceptable; (4) correction is inappropriate if treatment results in blood glucose outside of the target range; and (5) failure to treat reference glucose concentrations higher than 240 mg/dL is inappropriate. If these assumptions are valid, then for reference blood glucose over 70 mg/dL, predicted values between 110 mg/dL over and 60 mg/dL under the reference value are acceptable (in ''A'' or ''B'' areas of the grid). HAH spectra from NIR exposures of approximately 1800 mJ satisfy these criteria ($r^2=0.987$; RMSEP=23 mg/dL).

For reference concentrations less than 70 mg/dL, predictions of spectra from any safe or practical range of light exposures are thus far inadequate. There is a sharp discontinuity in acceptability at 70 mg/dL due to the Clarke grid requirement that predictions corresponding to reference values from 70 down to 58 mg/dL never more than 20% higher than the reference value, and predictions corresponding to reference values less than 58 mg/dL never more than 70 mg/dL. The smallest range of acceptable positive errors occurs at a reference concentration of 58 mg/dL, where the maximum acceptable positive error is 12 mg/dL. At 70 mg/dL, the 20% limitation means that error in predicted blood glucose must be less than 14 mg/dL. These small tolerances can be compared to the range of observed errors. For predictions of 17 HAH samples (using the 50-AAH PLS model on summed spectra equivalent to 150 s, ~15 000 mJ exposure), the root mean square error of prediction was 20.4 mg/dL. Thus, acceptable glucose measurements at very hypoglycemic levels may be difficult to achieve with Raman spectroscopy of aqueous humor even with high-energy exposures.

For practical purposes accurate glucose measurements below 70 mg/dL may not be necessary. Since patients with glucose in this range are usually symptomatic, a spectrometer reading predicting that blood glucose is ''low'' is probably adequate. Under such circumstances a patient can reassess his or her glucose level after correcting blood glucose with a meal.

System Performance

The SNR performance of the Raman spectrometer used in this paper was carefully measured so that its performance could be easily compared to other systems being utilized for this application. Six hundred cosmic ray free Raman spectra of a 5000 mg/dL glucose solution in water were acquired using 3 s, 100 mW exposures. The first group of 75 spectra were used to calculate the SNR for an exposure of 100 mW×3 s=300 mJ by dividing the average intensity across the 75 member set by the standard deviation at each wave number shift. Then the intensities of the first and second set of 75 spectra were summed as a function of wave number shift and used to calculate the SNR for an exposure of 100 mW×6 s=600 mJ, and so on. The SNR as a function of Raman shift is shown for exposures ranging from 300 to 2400 mJ in Fig. 2. The graph shows that SNR increases with increasing exposure, but less so with each subsequent exposure increment.

Ocular Toxicity Issues

In spite of its advantage of accessibility for spectroscopic analysis, the eye has the disadvantage of risk for disabling injury if the light used as a spectroscopic probe is too intense. In the case of our Raman system, 785 nm was chosen because of its minimal absorption by the cornea and lens.[27,28] This optimizes transmission to and from the aqueous humor and minimizes the risk of damage to those tissues closest to the focal plane. NIR light has the additional advantage of causing purely thermal damage, which occurs when the tissue is heated 10–20 °C above ambient temperature.[29] There is no accumulated damage from photochemical toxicity, as is the case with shorter wavelengths.[30] Thus, it is safe to use repeatedly as long as thermal damage thresholds are not exceeded.

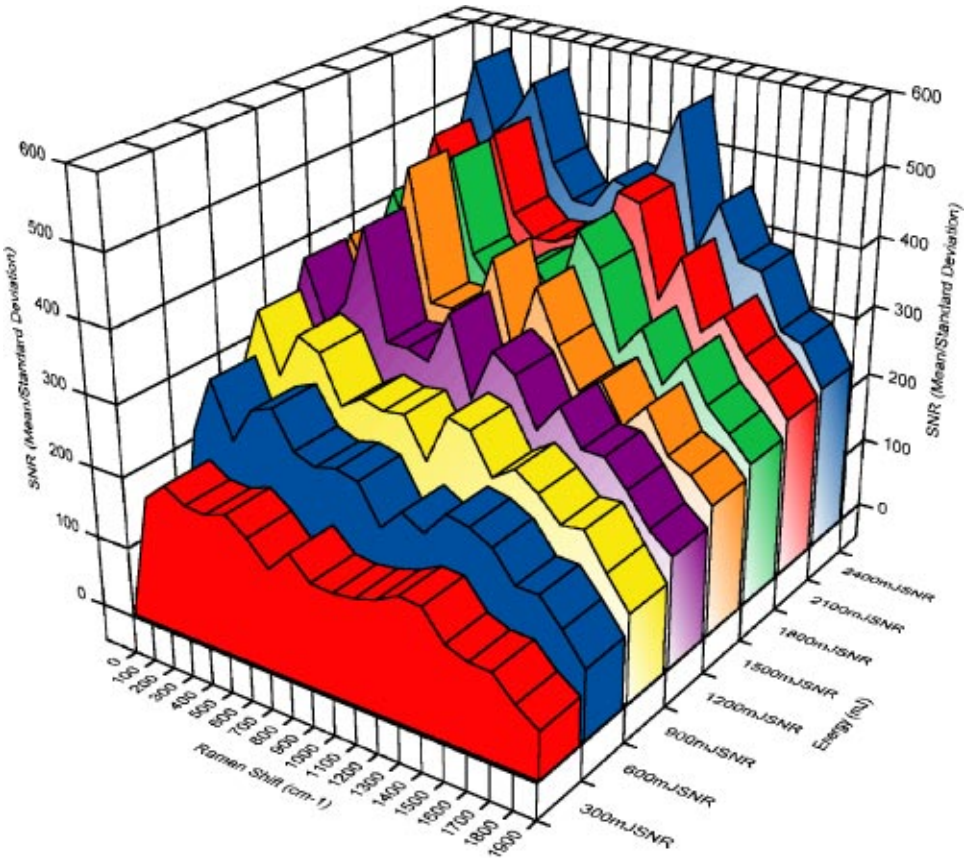

Fig. 2 SNR measurements as a function of Raman shift are shown for several energies of exposure. SNR increases with energy delivered to the sample. The average SNR across the 300–1500 cm^{-1} range for which the PLS model was developed was 163, 234, 287, 323, 338, 365, 399, and 441 for applied energies of 300, 600, 900, 1200, 1500, 1800, 2100, and 2400 mJ, respectively.

Absorption of NIR light is primarily by melanin containing tissue. Thus, the retina is at most risk for damage from our Raman system and the retinas of darkly pigmented individuals are at greater risk than those of lightly pigmented individuals.[31] The effective dose (ED) is the amount of energy required to produce a specified effect in 50% of an animal population. The International Commission on Non-Ionizing Radiation Protection (ICNIRP) and the American National Standards Institute (ANSI) set safe exposure limits of the eyes to laser light that are designed to be one tenth of the ED50 (specified effect=a retinal burn) from any wavelength of light.[32,33] These guidelines are based on ocular injury data from animal studies and can be modified based on a risk/benefit assessment of the laser delivery device. Unfortunately no prior studies exist that calculate the ED50 of NIR light near the wavelength that we are using.

In order to determine the ED50, we studied the effect of 20 s exposures of 785 nm light from our Raman system on the retinas of 23 pigmented rabbits. Intensities were chosen to bracket the anticipated intensity threshold for a burn with an emphasis on exposures likely to be just below the threshold. Six animals had both eyes exposed, with one eye randomly selected to receive power exposure estimated to be 10%–20% below the burn threshold, and the other eye 10%–100% above the burn threshold. In the 17 other animals only one eye was exposed. The unexposed eye served as a control. Color photographs and fluorescein angiograms were obtained on all eyes immediately following exposure and 48–72 h later. Two masked observers scored these photographs as to presence or absence of a burn. There was 100% agreement between these observers.

The laser beam spot size on the rabbit retina was calculated by multiplying the beam divergence (α=0.1069 rad) by the distance from the retina to the theoretical nodal point (Fig. 3). This nodal distance was determined by correcting the nodal distance from the reduced schematic rabbit eye with the measured axial lengths and refractive errors of the experimental rabbit eyes. The schematic rabbit eye has an axial length

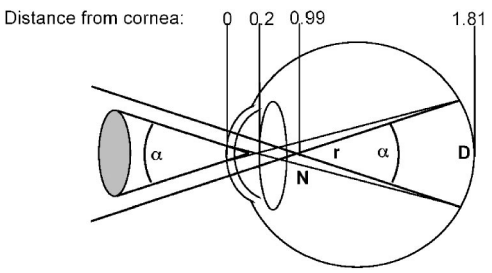

Fig. 3 Optical power density calculations are performed using a modified rabbit schematic eye. Rays converging on the eye at an angle α behave as if they emanate from node point **N** at the same angle. The diameter **D** of the spot on the retina can therefore by calculated by using the relation $\mathbf{D}=\mathbf{r}\boldsymbol{\alpha}$.

(L) of 18.1 mm and a nodal distance (r) of 9.9 mm with a total power (p) of 100.6 diopters.[34] The mean axial length of the experimental rabbit eyes was 16.96±0.46 mm. The mean refractive error (spherical equivalent) was 1.49±0.74 diopters. The average calculated spot size diameter (full width at half maximum) on the retina was 1.01±.02 mm. By virtue of its smaller eye, the spot size is smaller, while the retinal power density is higher, in the rabbit than in the human.

An estimate of ED50 with 95% confidence interval was obtained using logistic regression detailed in Stokes et al.[35] Both two-sided and one-sided confidence intervals were calculated. The one-sided confidence interval was narrower, as more exposures were below than above the burn threshold. This provided a better estimate of the clinically relevant lower limit of toxicity.

The ED50 for incident corneal power causing retinal damage was 100.09 mW (95% confidence lower limit: 84.09 mW [one-sided]; 80.96 mW [two-sided]). The ED50 for retinal power density was 12 548 mW/cm^2 (95% confidence lower limit: 10 752 mW/cm^2 [one-sided]; 10 401 mW/cm^2 [two-sided]).

The ICNIRP maximum permissible exposure (MPE) for corneal surface exposure to a continuous wave (cw) laser beam takes into account laser wavelength, the angular aperture of the source, and the time of exposure. For exposures in the wavelength range 700–1050 nm where thermal risk to the retina is of primary concern, power limits are gradually reduced for longer times. For 18 μs–100 s exposure to cw sources with apparent visual angles greater than 100 mrad (as with our Raman instrument), the maximum permitted corneal power density is reduced as a function of exposure time given by

$$P_{\mathrm{dc}} = 1.8(\alpha^2/150)10^{2(\lambda - 0.700)}t^{-1/4} \ \mathrm{mW/cm^2}, \qquad (1)$$

where P_{dc} is the corneal power density in mW/cm^2, α is the angular extent of the beam, λ is the wavelength of the laser excitation source in microns, and t is the exposure time in seconds.

For cw exposures times greater than 100 s (but less than 30 000 seconds), further reductions in power density are not required and the limits are determined by setting t to 100 s in Eq. (1) above.

The ICNIRP limits for retinal power densities were developed assuming a laser beam fills a fully dilated 7 mm diameter pupil. Therefore, the ICNIRP recommended limit for incident power on the cornea that can be transmitted to the retina is

$$P_r = P_{\mathrm{dc}}\pi D^2/4, \qquad (2)$$

where P_r is the power in milliwatts at the cornea, and the pupil diameter D is 7 mm. We can convert Eq. (2) above into an expression describing the equivalent safe power density limits on the retina, by dividing by the area of exposed retina. This can be performed for the specific case of our Raman instrument using a reduced human eye model in which the power of the cornea and intraocular lens are lumped into a single optical element with node point N and an effective focal length of 17.2 mm.[36] Since our instrument has a convergence angle of 106.9 mrad, and the node point of the model human eye is 1.72 cm from the retina, simple geometry can be used to show that the area of the exposed area of the typical human retina is 0.0265 cm^2. Using Eqs. (1) and (2), the ICNIRP power and power density limits for several exposure times can be calculated for the specific case of our instrument (see Table 1).

Table 1 Calculated ICNIRP maximum permissible optical exposure for 785 nm light using the reduced schematic human eye.

Exposure time (s)	Corneal power density limit (mW/cm^2)	Corneal power limit (mW)	Retinal power density limit (mW/cm^2)
1	202.8	78.1	2940.1
10	114.1	43.9	1653.3
20	95.9	36.9	1390.3
100	64.1	24.7	929.6

The retinal power density MPE for 785 nm light for humans is therefore about ten-fold less than the actual ED50 for retinal power density in rabbits with a 20 s exposure, just as anticipated by ICNIRP. The recommended human corneal power limits are only about one-third of the corneal power ED50 for rabbits. This is consistent with the larger size of the human eye resulting in lower retinal power densities in humans than in rabbits for a given corneal exposure.

We did not calculate the corneal power densities for our rabbit exposures. They would no doubt greatly exceed the ICNIRP recommended limits due to the small spot size on the cornea from our instrument. This is largely irrelevant since the limits are designed to prevent retinal damage anticipating that this would be the dose-limiting toxicity. ICNIRP did not anticipate laser delivery systems such as ours focused in the aqueous humor. This raises the question: Could corneal or lens thermal damage result from NIR light focused in the aqueous humor even if it is insufficient to cause retinal damage because of its defocused state in the plane of the retina?

The estimated transmission of 785 nm light by the cornea, aqueous humor, lens, and vitreous is 95%.[37] Five percent of the light is absorbed or reflected by the ocular media. Given the index of refraction of the cornea of 1.376, one can calculate the reflected light is 2.5% assuming the incidence angle is normal to the surface. Thus the entire ocular media absorbs only 2.5% of the light. If fully half of this is absorbed each by the lens and cornea, 1.25% of the total light is absorbed by each of these structures. The retinal pigment epithelium absorbs approximately 35% of 785 nm light.[31] Thus, one might anticipate that the ED50 power density for corneal burns would be 30 times that of the retina, and lasers focused near the cornea could result in corneal damage while sparing the retina because of the vast difference in spot size at those two tissue planes. Several issues complicate such calculations. First, NIR energy absorbed by the retina is concentrated in the single cell layer thickness of the retinal pigment epithelium, whereas that absorbed by the cornea and lens is dispersed throughout the entire thickness of those two structures. (The cornea is 500 μm thick; the lens is 3600 μm; the retinal pigment epithelium is 7–10 μm.) Thus the power density (by

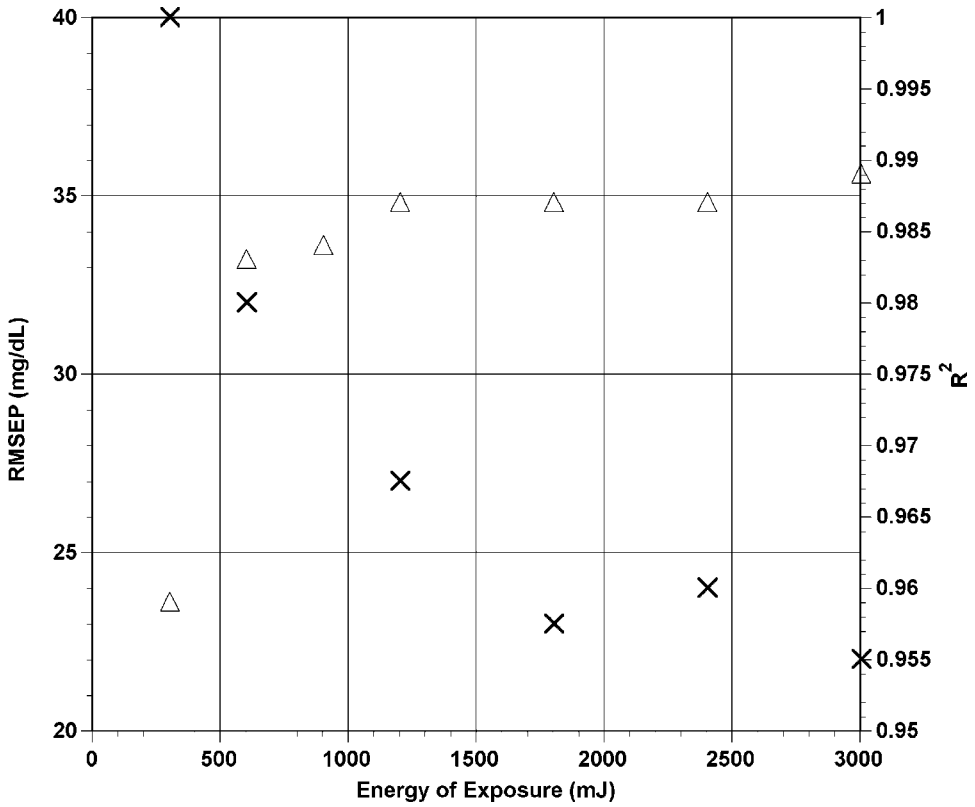

Fig. 4 Root mean squared error of prediction (X=RMSEP) and the correlation coefficient ($\Delta = R^2$) are plotted as a function of optical dose (mJ). At 800 mJ, R^2 plateaus at 0.99 while the nadir of RMSEP occurs at 1600 mJ. A variable number of consecutive low energy exposures can be applied to achieve the required clinical accuracy required while minimizing the total optical dose delivered to the patient.

tissue volume) is several hundredfold less in the cornea and lens than in the retina. Second, because of its high blood flow, the retina has a much higher cooling capacity than other structures of the eye. Thus the actual ED50 for corneal or lens damage from NIR light awaits experimental validation. However, we examined all our rabbits for cornea or lens damage with a microscope 48–72 h after exposure in our retinal toxicity experiment. No such injury was seen, even in rabbits exposed to 200 mW (~2300 W/cm^2) incident light on the cornea. It is therefore unlikely that corneal damage can occur with exposure powers below the threshold for retinal damage in the described system. It remains to be seen if histologic evidence of thermal injury to the cornea can be detected.

Tradeoffs in Performing Optical Glucose Measurements

Figure 4 shows a graph of r^2 and RMSEP as a function of optical dose (mJ) that were obtained using 17 samples of HAH. As one would expect, greater measurement accuracy is obtained as the available signal to noise ratio is increased as seen in Fig. 2. The instrument produces accuracies ranging from 40 to 23 mg/dL as total energy dose is varied from 300 to 1800 mJ. Since the required accuracy of glucose monitoring devices as established by the Clarke grid is dependent on the actual value of glucose being measured, applied energy could be adaptively controlled through variable number serial exposures. An initial exposure of relatively low energy (e.g., 300 mJ) could be applied to determine if glucose levels are in the higher range where accuracy requirements are less stringent. The acquisition could be stopped if glucose levels were indeed elevated where accuracy is expected to be within the "A or B" range of the Clarke grid even at low energy exposures. When initial exposures provide a lower glucose concentration estimate, additional exposures could be serially delivered within eye-safe limits to obtain the accuracies clinically indicated by the Clarke grid.

The trade space between exposure time and retinal power density (on a schematic human eye) is shown for our system in Fig. 5, with boundary conditions dictated by maximum measurement time tolerable by the patient, acceptably low likelihood of optical toxicity, and energy dose contours proportional to glucose measurement accuracy. The maximum tolerable measurement time (from the patient's perspective) was arbitrarily chosen to be 100 s. ICNIRP exposure limits referred to the retina of the schematic eye were selected to be the upper bound for optical dose (minimal likelihood of optical toxicity), by using the current instrument optics, and focusing 1 mm below the corneal surface. The graph shows a series of constant energy contours representing where the current instrument can operate. As discussed, total dose could be applied in an iterative fashion (e.g., 300 mJ increments) to achieve A or B region accuracy standards established by the Clarke grid. Therefore, triangular regions of operation are established given the boundaries of ICNIRP maximum retinal power density, maximum tolerable measurement time, and minimum energy producing a "useful" measurement within

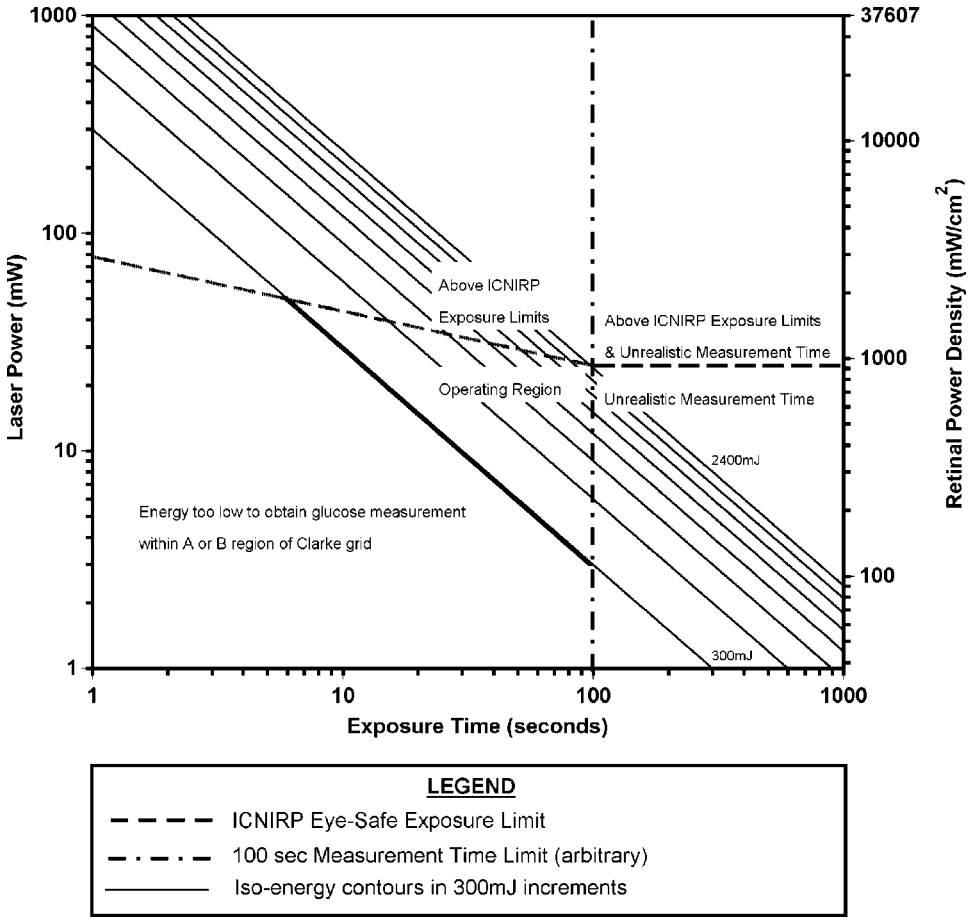

Fig. 5 The operating region of NIR Raman-based optical glucometers fall within a triangular region of the log–log plot of applied laser power versus exposure time. The upper bound side of the triangle is the maximum exposure limits recommended by ICNIRP in terms of optical power density. Iso-energy contour lines passing through the operating region are believed to be eye-safe when using an excitation source with an optical wavelength of 785 nm.

any region on the Clarke grid. Adaptive algorithms operating within these regions could be developed to optimize a cost function that achieves required measurement accuracies as a function of applied power, measurement time, and likelihood of optical toxicity.

Instrument Design Considerations

The graph shown in Fig. 5 is specific to the current instrument's capabilities based upon its sensitivity, stability, and optical design. Some improvements may be implemented to allow additional flexibility. For example, doubling the diameter of the 0.7 mm laser beam incident on the 20× focusing objective would reduce the power density incident on the retina effectively multiplying each iso-enenegy contour shown in Fig. 5 by 4, vastly increasing the flexibility in performing accurate, safe, and convenient optical glucose measurements. One caveat to this approach is that the Raman light collected by the confocal aperture would be reduced slightly (since the depth of field of the instrument would be reduced). Simply increasing the diameter of the confocal aperture could compensate for this reduction in signal.

Safety features will have to be designed into the instrument to control depth of focus and centering of the light beam (thereby avoiding thermal damage to the iris) prior to routine use in humans.

Conclusion

Numerous approaches are being used to develop technology that will permit noninvasive measurement of blood glucose in humans. Thus far, studies using Raman spectroscopy to predict glucose concentration in the aqueous humor of the eye have demonstrated reasonable accuracy of glucose measurement within clinically relevant ranges with partial least squares analysis and artificial aqueous humor training sets. The power necessary to achieve this is within an acceptable range of safety and patient tolerability. Future work will focus on demonstrating safety and efficacy in humans, improving signal-to-noise, miniaturization, and determining the equilibration relationship between blood glucose and aqueous humor glucose.

Acknowledgment

The Jet Propulsion Laboratory, a division of the California Institute of Technology and Childrens Hospital Los Angeles carried out this research under a contract with the National Aeronautics and Space Administration (NASA).

References

1. G. F. Cahill, Jr., J. S. Soeldner, G. W. Harris, and R. O. Foster, ''Practical developments in diabetes research,'' *Diabetes* **21**, 703–712 (1972).
2. P. G. Steffes, ''Laser-based measurement of glucose in the ocular aqueous humor: an efficacious portal for determination of serum glucose levels,'' *Diabetes Technol. Ther.* **1**, 129–133 (1999).
3. R. J. McNichols and G. L. Coté, ''Optical glucose sensing in biological fluids: An overview,'' *J. Biomed. Opt.* **5**, 5–16 (2000).
4. O. S. Khalil, ''Spectroscopic and clinical aspects of noninvasive glucose measurements,'' *Clin. Chem.* **45**, 165–177 (1999).
5. R. D. Lasker, ''The diabetes control and complications trial—Implications for policy and practice,'' *N. Engl. J. Med.* **329**, 1035–1036 (1993).
6. National Institute of Diabetes and Digestive and Kidney Disorders, *The Diabetes Control and Complications Trial*, NIH Publication No. 97-3874, National Institutes of Health, Bethesda (1994).
7. http://www.cdc.gov/diabetes/pubs/pdf/ndfs_2003.pdf
8. K. J. Ward, D. M. Haaland, M. R. Robinson, and R. P. Eaton, ''Postprandial blood glucose determination by quantitative mid-infrared spectroscopy,'' *Appl. Spectrosc.* **46**, 959–965 (1992).
9. M. J. Goetz, Jr., G. L. Coté, R. Erckens, W. March, and M. Motamedi, ''Application of a multivariate technique to Raman spectra for quantification of body chemicals,'' *IEEE Trans. Biomed. Eng.* **42**, 728–731 (1995).
10. A. J. Berger, Y. Wang, and M. S. Feld, ''Rapid, noninvasive concentration measurements of aqueous biological analytes by near-infrared Raman spectroscopy,'' *Appl. Opt.* **35**, 209–212 (1996).
11. F. M. Ham, I. N. Kostanic, G. M. Cohen, and B. R. Gooch, ''Determination of glucose concentrations in an aqueous matrix from MIR spectra using optimal time-domain filtering and partial least-squares regression,'' *IEEE Trans. Biomed. Eng.* **44**, 475–485 (1997).
12. L. Zhang, G. W. Small, and M. A. Arnold, ''Multivariate calibration standardization across instruments for the determination of glucose by Fourier transform near-infrared spectrometry,'' *Anal. Chem.* **75**, 5905–5915 (2003).
13. G. L. Coté, R. M. Lec, and M. V. Pishko, ''Emerging biomedical sensing technologies and their applications,'' *Sensors* **3**, 251–266 (2003).
14. G. L. Coté, ''Noninvasive and minimally-invasive optical monitoring technologies,'' *J. Nutr.* **131**, 1596S–1604S (2001).
15. M. S. Borchert, M. C. Storrie-Lombardi, and J. L. Lambert, ''A noninvasive glucose monitor: Preliminary results in rabbits,'' *Diabetes Technol. Ther.* **1**, 145–151 (1999).
16. S. Y. Wang, C. E. Hasty, P. A. Watson, J. P. Wicksted, R. D. Stith, and W. F. March, ''Analysis of metabolites in aqueous solutions by using laser Raman spectroscopy,'' *Appl. Opt.* **32**, 925–929 (1993).
17. R. J. Erckens, M. Motamedi, W. F. March, and J. P. Wicksted, ''Raman spectroscopy for non-invasive characterization of ocular tissue: Potential for detection of biological molecules,'' *J. Raman Spectrosc.* **28**, 293–299 (1997).
18. J. M. Khosrofian and B. A. Garetz, ''Measurement of a Gaussian laser beam diameter through the direct inversion of knife-edge data,'' *Appl. Opt.* **22**, 3406–3410 (1983).
19. J. L. Lambert, J. M. Morookian, S. Sirk, and M. S. Borchert, ''Measurement of aqueous glucose in a model anterior chamber using Raman spectroscopy,'' *J. Raman Spectrosc.* **33**, 524–529 (2002).
20. M. L. Sears, ''Dynamics of ocular fluids and control of intraocular pressure: formation of aqueous humor,'' in *Principles and Practice of Ophthalmology*, D. M. Albert and F. A. Jakobiec, Eds., W. B. Saunders, Philadelphia (1994).
21. R. G. Brereton, *Chemometrics, Data Analysis for the Laboratory and Chemical Plant*, Wiley, Chichester (2003).
22. W. L. Clarke, D. Cox, L. A. Gonder-Frederick, W. Carter, and S. L. Pohl, ''Evaluating clinical accuracy of systems for self-monitoring of blood glucose,'' *Diabetes Care* **10**, 622–628 (1987).
23. S. Pohjola, ''The glucose content of the aqueous humor in man,'' *Acta Ophthalmol. Suppl.* **88**, 11–80 (1966).
24. W. F. Schrader, R. S. Grajewski, P. Meuer, and W. Kiefer, ''The glucose content of the aqueous humor compared with capillary blood in man,'' *Invest. Ophthalmol. Visual Sci.* **41**, S77 (2000).
25. B. D. Cameron, J. S. Baba, and G. L. Coté, ''Measurement of the glucose transport time delay between the blood and aqueous humor of the eye for the eventual development of a noninvasive glucose sensor,'' *Diabetes Technol. Ther.* **3**, 201–207 (2001).
26. B. Rabinovitch, W. F. March, and R. L. Adams, ''Noninvasive glucose monitoring of the aqueous humor of the eye. Part I. Measurement of very small optical rotations,'' *Diabetes Care* **5**, 254–258 (1982).
27. T. J. T. P. Van den Berg and H. Spekreijse, ''Near infrared light absorption in the human eye media,'' *Vision Res.* **37**, 249–253 (1997).
28. D. G. Pitts, L. L. Cameron, J. G. Jose et al., ''Optical radiation and cataracts,'' in *Optical Radiation and Visual Health*, M. Waxler and V. M. Hitchins, Eds., CRC Press, Boca Raton, FL (1986).
29. W. T. Ham, J. J. Ruffolo, H. A. Mueller, and D. P. Guerry, ''The nature of retinal radiation damage: Dependence on wavelength, power level and exposure time,'' *Vision Res.* **20**, 1105–1111 (1980).
30. J. Mellerio, ''Light effects on the retina,'' in *Principles and Practice of Ophthalmology*, D. M. Albert and F. A. Jakobiec, Eds., Saunders, Philadelphia (1994).
31. W. J. Geeraets, R. C. Williams, G. Chan, W. T. Ham, D. P. Guerry, and F. H. Schmidt, ''The relative absorption of thermal energy in retina and choroids,'' *Invest. Ophthalmol.* **1**, 340–347 (1962).
32. International Commission on Non-Ionizing Radiation Protection, ''Revision of guidelines on limits of exposure to laser radiation of wavelengths between 400 nm and 1.4 μm,'' *Health Phys.* **79**, 431–440 (2000).
33. American National Standards Institute, *American National Standards for the Safe Use of Lasers: ANSI Z-136.1-2000*, Laser Institute of America, Orlando, FL (2000).
34. A. A. Hughes, ''A schematic eye for the rabbit,'' *Vision Res.* **12**, 123–138 (1972).
35. M. E. Stokes, C. S. Davis, and G. G. Koch, *Categorical Data Analysis Using the SAS System*, SAS Institute, Cary, NC (1995).
36. K. Ogle, *Optics*, pp. 156–157, C. C. Thomas, Springfield (1968).
37. W. J. Geeraets and E. R. Berry, ''Ocular spectral characteristics as related to hazards from Lasers and other light sources,'' *Am. J. Ophthalmol.* **66**, 15–20 (1968).